Experimental investigation of the oxidative ageing mechanisms in bitumen

Pipintakos, Georgios; Vincent Ching, H. Y.; Soenen, Hilde; Sjövall, Peter; Mühlich, Uwe; Van Doorslaer, Sabine; Varveri, Aikaterini; Van den bergh, Wim; Lu, Xiaohu

DOI
10.1016/j.conbuildmat.2020.119702

Publication date
2020

Document Version
Final published version

Published in
Construction and Building Materials

Construction and Building Materials 260 (2020) 119702

Contents lists available at ScienceDirect

Construction and Building Materials

journal homepage: www.elsevier.com/locate/conbuildmat

Experimental investigation of the oxidative ageing mechanisms in bitumen

Georgios Pipintakos [a,*], H.Y. Vincent Ching [b], Hilde Soenen [c], Peter Sjövall [d], Uwe Mühlich [a], Sabine Van Doorslaer [b], Aikaterini Varveri [e], Wim Van den bergh [a], Xiaohu Lu [f]

[a] University of Antwerp, EMIB Research Group, Groenenborgerlaan 171, Antwerp 2020, Belgium
[b] University of Antwerp, Bimef Research Group, Universiteitsplein 1, Wilrijk 2610, Belgium
[c] Nynas NV, Groenenborgerlaan 171, Antwerp 2020, Belgium
[d] RISE Research Institutes of Sweden, 4P.O. Box 857, SE-501 15 Borås, Sweden
[e] Delft University of Technology, Pavement Engineering, Stevinweg 1, Delft 2628 CN, Netherlands
[f] Nynas AB, Raffinaderivägen 21, Nynäshamn SE 149 82, Sweden

HIGHLIGHTS

- EPR provides evidence for carbon-centred radical formation during exposure of bitumen to oxygen.
- TOF-SIMS demonstrates an increase of SO_x^--, HO_x^--, NO_x^--organics because of ageing.
- A fast- and a slow-rate phase for ageing can be distinguished with FTIR.
- EPR also shows that vanadyl-porphyrin species remain unchanged during ageing.

ARTICLE INFO

Article history:
Received 14 February 2020
Received in revised form 12 May 2020
Accepted 26 May 2020
Available online 28 June 2020

Keywords:
Bitumen
Ageing mechanisms
EPR
FTIR
TOF-SIMS

ABSTRACT

Oxidative ageing in bituminous materials is considered one of the most important factors for distress types in road applications. This paper aims to offer insights into the validity of commonly held beliefs regarding the oxidation phases of ageing in bitumen, the fast- and the slow-rate phase, and explore the main oxidation products formed upon ageing. In order to evaluate possible differences between bitumen types, the penetration grade as well as the bitumen production process was varied. Thus, the ageing of three different binders was first studied by Fourier-Transform Infrared (FTIR) and Electron Paramagnetic Resonance (EPR) spectroscopy. The formation of oxygen-containing molecular structures on the bitumen surface during ageing was studied with Time-of-Flight Secondary Ion Mass Spectrometry (TOF-SIMS). The results of FTIR reveal a gradual increase of sulfoxides upon ageing, while the EPR results show an increase of organic carbon-centred radicals. In parallel, TOF-SIMS results provide evidence for an increase of oxygenated compounds, such as SO_x^-, HO_x^- and NO_x^--containing compounds. It appears also that paramagnetic metal species, such as vanadyl-porphyrins, are insusceptible during ageing. Overall, the findings of this study are in agreement with a mechanism comprising two rate-determining phases and support the formation of different oxygenated products. It is believed that the experimental approach used in this work may contribute further to an improved understanding of the ageing mechanisms in bitumen.

1. Introduction

Bituminous binders are composed of a variety of organic molecules consisting of about 85% carbon, 10% hydrogen, heteroatoms such as nitrogen (0–2%), oxygen (0–2%), sulfur (0–9%) and traces of metals such as vanadium, iron and nickel [1,2]. Among the myriad of chemical functional groups of neat bitumen are the hydroxyl groups of phenols, imino groups of pyrrolic compounds, as well as carbonyl groups of ketones, carboxylic acids and 2-quinolones [3,4]. The heteroatoms in bituminous organic molecules not only modulate the polarity but also constitute chemical functional groups that can react and change. In particular, a wide variety of sulfur-containing compounds occurs preferentially within bituminous binders, such as sulfides, disulfides, sulfoxides, ring

* Corresponding author.
E-mail address: Georgios.Pipintakos@uantwerpen.be (G. Pipintakos).

https://doi.org/10.1016/j.conbuildmat.2020.119702
0950-0618/

compounds (thiophenes, benzothiophenes and dibenzothiophenes) and their alkyl derivatives [5].

Previous studies have demonstrated the significance of bitumen chemistry as it can assist in the unravelling of the oxidative ageing mechanisms in bitumen [6]. More specifically, ageing of bitumen is a process of autoxidation as the binder reacts with oxygen, generating new compounds that may continue to react with oxygen. To date, a number of studies support that during the ageing process, the active functionalities of bitumen molecules are decomposed through the oxidative dehydrogenation of polycyclic perhydroaromatics generating intermediate hydroperoxides [7,8]. Through the years, different mechanisms have been proposed to describe this phenomenon ranging from an oxycyclic reaction mechanism [9] up to a dual sequential binder oxidation mechanism [4,10]. According to the latter, two major oxidation routes may exist, namely the chemically distinct "fast-spurt" and "slow/long-term" routes [6,10–12]. This idea has gained considerable support since a direct link with the asphalt production stages can be established [13].

Among other factors, it should be acknowledged that the temperature may vary between different asphalt mixture applications (hot, warm, cold) or stages of the service life. Thus, certain standardised ageing protocols exist in order to simulate the different stages. It has been reported previously that the temperature during the short-term ageing in production stage has a stronger effect on the intensity of oxygenated products than the temperature during the long-term ageing in service life [14,15]. Moreover, the literature emphasises that an increase of 10 °C may double the reaction rate and a relatively high temperature may destroy certain microstructures of the polar species [6]. Care should be taken when reviewing these mechanisms by taking into account the corresponding thermal history varying per asphalt application. Nevertheless, the ageing mechanisms will remain somewhat similar independently of the thermal history and they may be affected only in terms of quantity of products and reaction rate.

The studies presented so far provide evidence that the ageing-produced ketones and carboxylic acids are of high polarity, generating strong associations, expressed through their Van der Waals forces. Subsequently, the polar compounds of bitumen may interact with each other [16]. Possible chemical changes could induce stronger interactions and change the bitumen microstructure which may have implications in the mechanical behaviour. Given this, there is a growing body of evidence that an increase in apparent molecular weight due to increased molecular interactions can reduce the mobility of molecules to flow which, in turn, will influence the bitumen rheology [17–20]. Eventually, there is a widespread recognition that the severity of ageing can be tracked by capturing the change in certain functional groups [13,18,19,21,22].

It appears that experimental validation of the underlying mechanisms has been confined primarily to sulfoxide and carbonyl formation. Considerable research has been devoted to the determination of these functional groups via chemical analysis such as Fourier-Transform Infrared spectroscopy (FTIR) [14,21,22]. When it comes to the fractions of bitumen, previous studies were also limited to the explanation that a sequential reaction, of aromatic to resin and finally to asphaltene fraction, takes place [23–25]. No further evidence for the mechanisms behind these changes and the accompanied reasoning has been provided apart from microstructural changes observed with the use of microscopy [26–29]. Challenges arise when specific products of ageing in bitumen are needed to be confirmed experimentally.

This study addresses a number of questions regarding the ageing mechanisms of bitumen. An important issue is the validation of the previously proposed oxidation schemes. This was achieved by utilising a number of spectroscopic techniques. In particular, support was provided by FTIR, EPR and TOF-SIMS spectroscopy. Links between the results of the three techniques under predefined oxidation time and temperature, finally, review certain hypotheses for the ageing mechanisms of bitumen.

2. Materials and methods

2.1. Materials and ageing treatment

Three bituminous binders were used as specified in Table 1, namely, a hard binder A and two soft binders B and C. Binders A and B originate from a wax-free crude oil, and differ only in the degree of distillation processing. Binder C is a visbroken residue, containing natural wax (crystallisable compounds) and coming from a different crude oil.

To simulate the oxidative ageing of the three binders, a modified thin film oven test (M−TFOT) was used: a binder film of approximately 1 mm thick was aged in an oven at 50 °C, for the FTIR and the TOF-SIMS measurements. That was not the case for the EPR measurements where binder films of thickness 3–5 mm were aged directly in polypropylene tubes. All the analyses were performed without prior sample mixing as additional heating may have a considerable effect on the oxidation process.

In all cases the film thickness was kept minimum in order to exclude, as much as possible, the diffusion effect from the coupled reaction–diffusion phenomenon of ageing. By minimising the film it is assumed that the diffusion effect will be eliminated and primarily oxidation will be the dominating process [30–32]. Instrumental constraints resulted in thicker films for the EPR analyses which may have experienced an increased diffusion. It should be noted that the EPR analyses measured the entire bitumen sample, therefore the number of spins derived from the EPR spectra were divided by the exact mass of the sample in order to extract a fair comparison value independently of the small fluctuation of thickness compared to FTIR and TOF-SIMS films.

All the ageing tests were conducted at 50 °C, as at this temperature a fast- and a slow-rate reaction can be clearly differentiated. Additionally, at this low temperature the decomposition of sulfoxides can be eliminated [6]. For the FTIR and EPR measurements, tests were conducted after several ageing time intervals, while for TOF-SIMS tests were conducted at two ageing times; the starting point with ageing time zero and after 8 days. These ageing times were derived from preliminary FTIR and EPR findings for a prolonged ageing time up to 56 days. A graphical summary including the main outcomes for each technique is presented in Fig. 1.

2.2. Spectroscopic techniques

2.2.1. Attenuated total reflectance-fourier transform infrared (ATR-FTIR)

The FTIR analysis was performed with a Thermo Scientific Nicolet iS10 FTIR spectrometer equipped with an Attenuated Total Reflectance (ATR) fixture and a Smart Orbit Sampling Accessory. At least three replicas were measured per ageing time interval. The collected spectra were acquired with 32 repetitive scans and ranged from 400 cm^{-1} to 4000 cm^{-1} with a resolution of 4 cm^{-1}.

In this study, a widely accepted protocol for the determination of the normalised intensity of certain functional groups was followed [21]. More specifically, the areas around certain peaks, as depicted for exemplary spectra of bitumen A in Fig. 2, were calculated. To do this, a baseline is introduced based on the limits of each band given in Table 2 and the area that is enclosed is computed based on the trapezoidal rule that approximates a definite integral. The focus here was exclusively on sulfoxides, which are more prone to be produced during oxidation at lower temperatures, like the one used (50 °C). For the quantification of the nor-

Table 1
Properties of the bituminous binders.

Material	Property	Binder			Test Method
Bitumen		A	B	C	
	Penetration 25 °C (0.1 mm)	16	189	190	EN1426
	Softening point (°C)	61.1	37.5	39.2	EN1427
	Penetration index, Ip	−1.06	−1.46	−0.63	EN12591
	Viscosity 135 °C (mm^2/s)	1285	203	N/D	EN12595

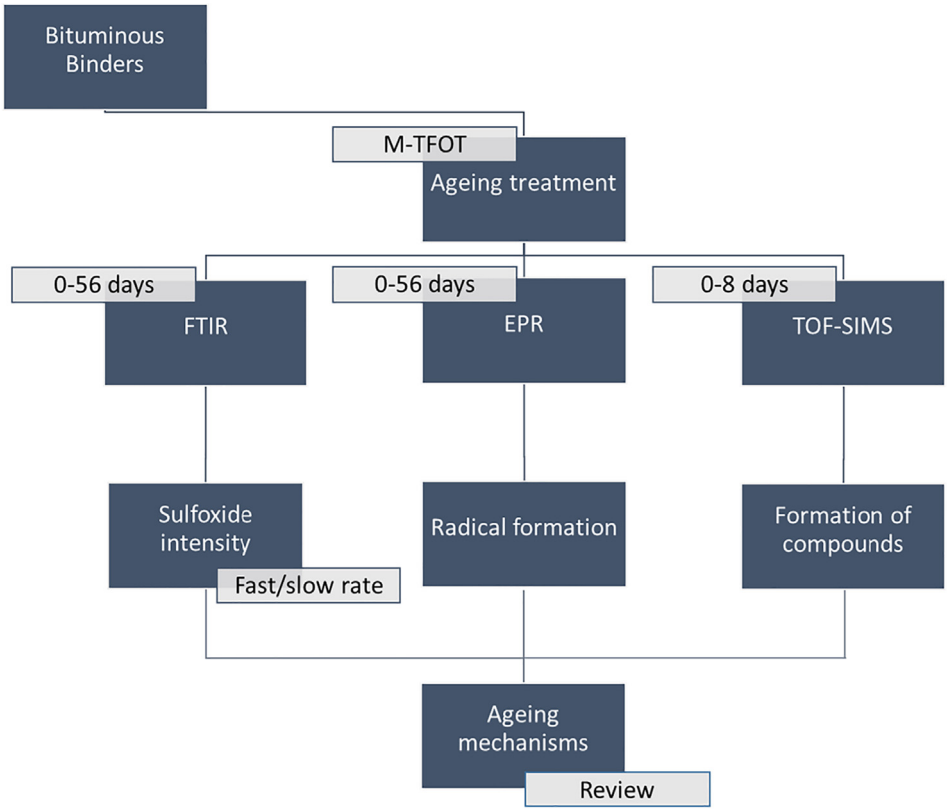

Fig. 1. Flowchart of the experimental part and objectives.

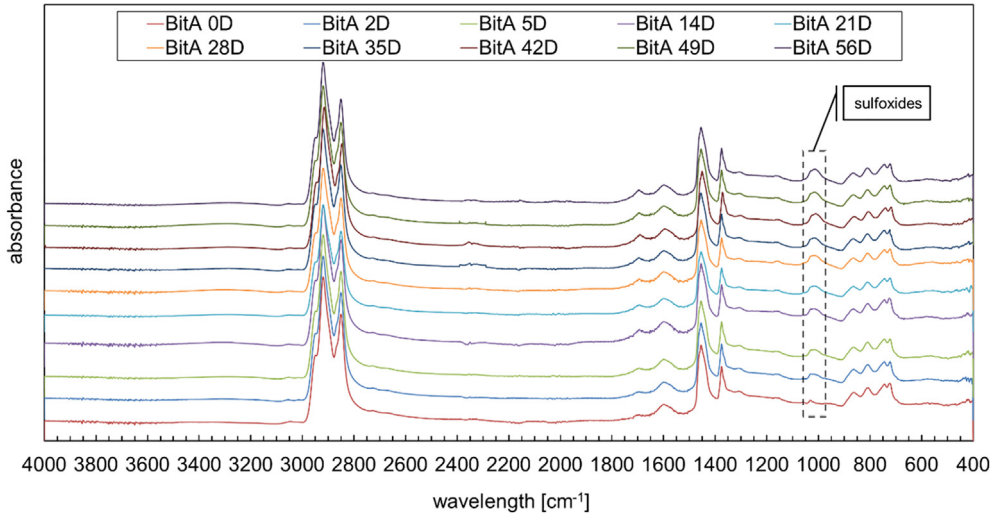

Fig. 2. Evolution with ageing time (0–56 days) for exemplary FTIR spectra of bitumen A.

Table 2
Band limits of the utilised FTIR functional groups.

Functional group	Bond vibration	Band limits for baseline (cm^{-1})	Area around peak n, (A_n)
Long Chains	$(CH_2)_n$ rock (n ≥ 4) bending	734–710	724
Aromatic structures	C = CH adjacent out of plane bending	783–734	743
Aromatic structures	C = CH adjacent out of plane bending	838–783	814
Aromatic structures	C = CH singlet out of plane bending	912–838	864
Sulfoxides	S = O stretching	1047–995	1030
Branched aliphatic structures	CH_3 symmetric bending	1390–1350	1376
Aliphatic structures	CH_3 asymmetric bending	1525–1395	1460
Aromatic structures	C = C stretching	1670–1535	1600
Carbonyls	C = O stretching	1753–1660	1700
Alkyl groups	C–H symmetric stretching	2880–2820	2862
Alkyl groups	C–H asymmetric stretching	2990–2880	2953

malised ageing intensity of sulfoxides, Equation 1 is applied. Despite the applied normalisation method, upon oxidation, discrepancies due to changes in the refractive index and subsequently in the effective path length controlled by the depth of penetration of the evanescent wave into the sample, may still arise. These effects, if present, are in the best scenario negligible.

$$\text{Normalised sulfoxide intensity} = \frac{A_{1030}}{\sum_{n=1}^{N}} \quad (1)$$

2.2.2. Electron paramagnetic Resonance (EPR)

EPR is a spectroscopic technique able to identify paramagnetic centres and molecules in a material, i.e. the components containing unpaired electrons. It is particularly useful to characterise organic radicals and transition-metal ions. Therefore, continuous-wave (cw) EPR spectra of aged and unaged bitumen samples were recorded with a Bruker Elexsys E680 spectrometer mounted with an ER 4102ST TE102 mode resonator working at ~ 9.75 GHz (X-band). Polypropylene Eppendorf tubes were used as sample holders ensuring that the total material quantity did not overfill the cavity. Preliminary measurements on the unaged binder A showed a two-component EPR spectrum consisting of contributions of a vanadyl centre (VO^{2+}, $S = 1/2$) and an organic carbon-centred radical. The former is characterised by an axial powder pattern with typical hyperfine splitting due to the interaction of the electron with the ^{51}V nucleus ($I = 5/2$), and the latter gives rise to an unresolved single line close to the free electron value ($g_e = 2.0023$) (Fig. 3a). This was also the case for binder B and C. Power saturation measurements showing different relaxation rates (Fig. 3b) confirmed the presence of the two species. For all subsequent measurements, 0.5 mW was chosen, because this was close to the highest microwave power level before either species became saturated (i.e. signal intensity vs $\sqrt{}$microwave power was linear, Fig. 3b). Simulation of the experimental spectra with Matlab2018b using the EasySpin-6.0 module [33], gave the EPR parameters of the two species (Table 3) as well as the relative amounts of spins between the two ('weights').

The EPR parameters of the observed VO^{2+} centres are consistent with those of VO^{2+} porphyrin centres found in heavy crude oils [34,35], while the parameter of the radical signal has been previously postulated to be carbon-based [36]. For the ageing experiments, at least three replicas were measured per ageing interval with the centre field at 341 mT, sweep width of 20 mT, resolution of 2048 points, modulation amplitude of 0.1 mT and modulation frequency of 100 kHz over 2 scans. The number of spins in each sample was estimated by comparing the double integral of each spectrum with those of TEMPO (2,2,6,6-tetramethyl-1-piperidiny loxyl, a chemical compound used commonly as a structural probe for radicals' characterisation) in toluene solution standards. The number of VO^{2+} or organic radical spins in each sample was estimated by comparing the weights used in the spectral simulations. Division by the mass of the sample gave the number of spins per gram of sample given in Fig. 5.

2.2.3. Time-of-flight secondary ion mass spectrometry (TOF-SIMS)

The analysis principle of TOF-SIMS includes the bombardment of the sample surface with high-energy primary ions and analysis of the emitted (secondary) ions with respect to mass-to-charge ratio (m/z). The obtained mass spectra provide molecular information about the sample surface and imaging of specific ions is accomplished by scanning the primary ion beam over a selected analysis area and acquiring separate mass spectra in each pixel [37]. In principle, the selection of the number of pixels in the TOF-SIMS analyses, i.e. the number of data points within the analysis area, is based on the fact that the pixel size should be matched with the diameter of the primary ion beam.

Here, the TOF-SIMS analyses were conducted in a TOF-SIMS IV instrument (IONTOF GmbH, Germany) using 25 keV Bi_3^+ primary ions and low-energy electron flooding for charge compensation. The sample temperature was kept at −80 °C during analysis to prevent diffusion/segregation in the bitumen due to the vacuum environment of the TOF-SIMS instrument. Bitumen samples were deposited on silicon wafer substrates and subsequently allowed to cool down according to a special protocol [2]. Positive and negative ion spectra were acquired over analysis areas of 200 μm × 200 μm (128 × 128 pixels) or 500 μm × 500 μm (256 × 256 pixels) at three locations of each sample, with the instrument optimised for high mass resolution ($m/\Delta m \approx 3000$–6000). In the case of bitumen C, additional positive and negative ion data was acquired (i.e. high resolution images) with the instrument optimised for high image resolution (lateral resolution ≈ 0.5 μm).

3. Results and discussion

3.1. Dual-oxidation route

3.1.1. FTIR analyses

The results of FTIR analyses show a steep increase of the normalised sulfoxide intensity followed by a steady milder increase for all three binders (Fig. 4). Binders A and C were found to have almost completed the initial rapid increase at about 5 days, whereas binder B reached this transition point at about 2 days. It becomes apparent that at 8 days of controlled ageing the slow-rate oxidation reaction has been initiated for all the binders.

Given that sulfoxides are considered to be one of the end products of both a fast and a slow reaction [6], oxidation kinetics were approximated in the following way for the product evolution. Assuming pseudo first-order kinetics and that the rate of the slow reaction is rather small, the evolution of an end product P, of a dual-sequential oxidation mechanism, can be described by Equation (2):

$$P(t) = P_{f\infty}\left(1 - e^{-k'_s t}\right) + P_{s\infty k'_s t} + C \quad (2)$$

where $P(t)$ is the amount of product as function of time; $P_{f\infty}$ and $P_{s\infty}$ are amounts of product from the fast and slow reactions, respectively at the reaction endpoint; k'_f and k'_s are pseudo first

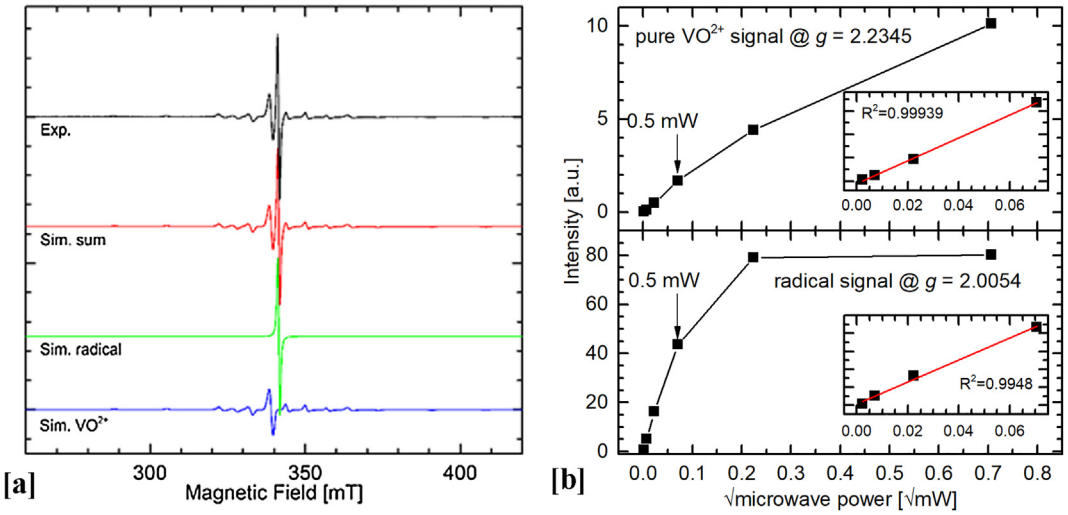

Fig. 3. Room temperature cw X-band EPR spectra of binder A with its simulations [a] and its signal intensity contrasted with square root of the power at different g-values, with insets showing a linear fit of selected powers [b].

Table 3
EPR parameters of the VO^{2+} and organic radical signal in binder A, B and C as determined by simulations of the room temperature cw X-band EPR spectra of the binders.

Binder	VO^{2+}				Radical
	$g_{\perp}$	$g_{\parallel}$	$A_{\perp}$ /mHz	$A_{\parallel}$/mHz	g_{iso}
A	1.9831 ± 0.0002	1.9616 ± 0.0002	160.4 ± 0.4	472.0 ± 1.5	2.0025 ± 0.0002
B	1.9831 ± 0.0003	1.9620 ± 0.0002	160.2 ± 0.5	471.9 ± 1.3	2.0026 ± 0.0003
C	1.9832 ± 0.0005	1.9610 ± 0.0008	160.0 ± 0.4	475.6 ± 1.2	2.0027 ± 0.0002

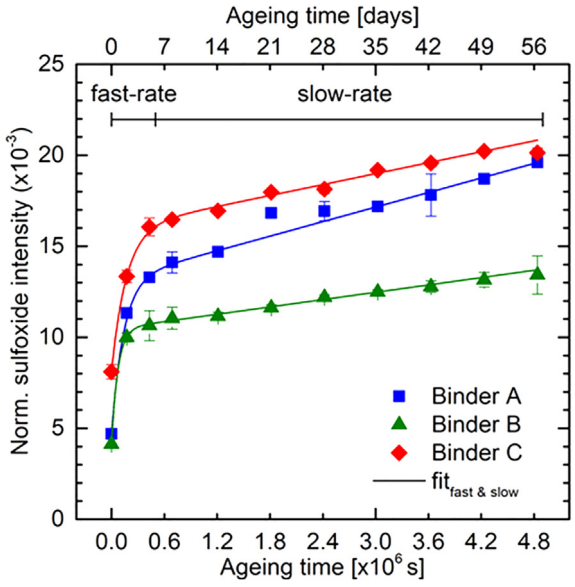

Fig. 4. Evolution of the FTIR normalised sulfoxide intensity over ageing time and the fitting used, based on a dual-sequential model [4,12].

order rate constants of the fast and slow reactions, respectively; and C is a constant [12]. The FTIR results for all three binders can be reasonably fitted to Equation (2) with their parameters given in Table 4.

From this analysis, $k_f^{'}$ was determined to be fastest for binder B, followed by A then C. Moreover, the percentile increase of the normalised sulfoxide intensity of the virgin binder up to the completion of the ageing treatment used here, was evaluated. This percentile increase demonstrates that binder A suffered from a harsher oxidation effect (317.88%) followed by binder B (224.52%) and C (148.39%), under the same ageing conditions.

Semi-quantitative methods to analyse the FTIR spectrum can be useful for identifying and characterising the evolution of specific oxidation products. Consistent with previous studies, this work demonstrated an initial rapid increase of sulfoxides followed by a slow-rate formation [4,6]. Hence, the kinetics of the normalised sulfoxide intensity can establish a simple way to distinguish different oxidation rates. At least, they can give a rough estimation for the two phases under the given ageing conditions.

3.1.2. EPR analyses

The time-dependent evolution of the EPR spectra of the three binders was investigated in the same timeframe as with the FTIR, up to 56 days. The graphs in Fig. 5a and 5b respectively, show the evolution of the organic carbon-centred radicals and VO^{2+} species over ageing time. Interestingly, in all cases the amount of VO^{2+} spins remained relatively constant as the samples were aged (a zeroth order line can be fitted with the error bars), while an increase was observed for the organic carbon-centred radicals (Fig. 5a). A comparison of the binders used in this study indicates also that the relative increase of organic carbon-centred radicals in binder C was about 1.5–2 times higher in comparison with binders A and B.

Although the results for the evolution of the carbon-centred radical EPR signal could also be fitted using Equation (2) (parameters given in Table 5), for each binder the contribution from the slow reaction term was almost negligible and for binder C it was even negative, which is contrary to a dual fast and slow production of end products model. These carbon-centred radicals are believed to be only produced and also subsequently consumed during the slow-rate phase. Since they are observable, their rate of production must be faster than their rate of consumption. In all cases, the evolution of the carbon-centred radical EPR signal is dominated by a

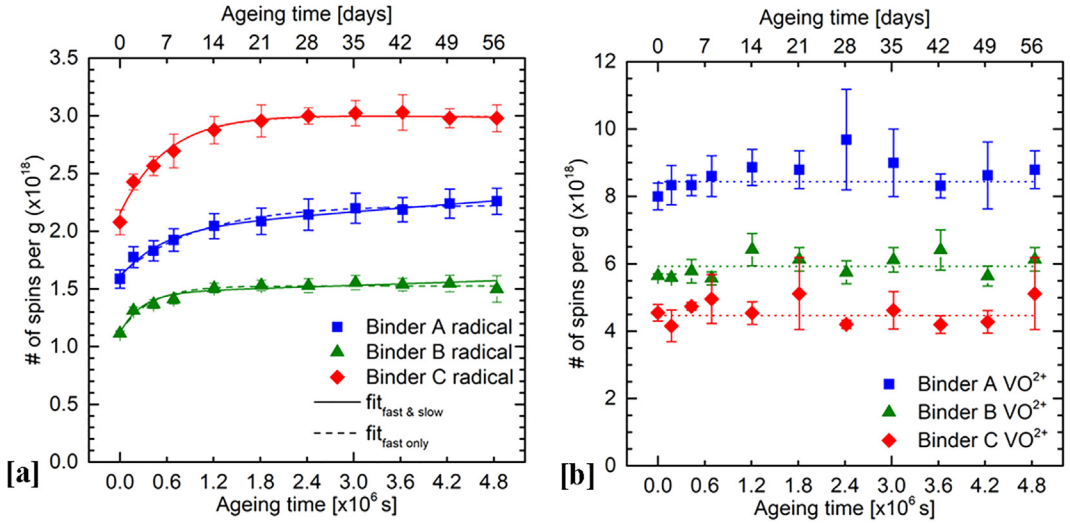

Fig. 5. Evolution of the carbon-centred radical and the used fitting, based on a dual-sequential or a fast reaction model [a] and VO^{2+} centres over ageing time [b].

Table 4
Parameters used for fitting Equation (2) to the FTIR normalised sulfoxide intensity and their R^2

Binder	$P_{f\infty}$ [$\times 10^{-3}$ a.u.]	k_f' [$\times 10^{-6}$ s^{-1}]	$P_{s\infty}k_s'$ [$\times 10^{-6}$ s^{-1}]	C [$\times 10^{-3}$ a.u.]	R^2
A	8.5 ± 0.2	7.3 ± 2.2	1.33 ± 0.03	4.69 ± 0.08	0.9997
B	6.3 ± 0.1	13.8 ± 1.5	0.67 ± 0.04	4.14 ± 0.01	0.9998
C	7.9 ± 0.7	5.9 ± 1.2	1.00 ± 0.07	8.12 ± 0.65	0.9827

Table 5
Parameters used for fitting the EPR spin counting of the radical signal and their R^2

Binder	Reaction(s)	$P_{f\infty}$ [$\times 10^{17}$ spins g^{-1}]	k_f' [$\times 10^{-6}$ s^{-1}]	$P_{s\infty}k_s'$ [$\times 10^{10}$ spins $g^{-1}s^{-1}$]	C [$\times 10^{17}$ spins g^{-1}]	R^2
A	Fast & slow	4.1 ± 0.5	1.9 ± 0.4	5.2 ± 1.4	16.0 ± 0.2	0.9862
	Fast only	6.1 ± 0.3	1.0 ± 0.1	N/A	16.0 ± 0.2	0.9772
B	Fast & slow	3.4 ± 0.4	3.7 ± 0.9	2.2 ± 1.4	11.0 ± 0.2	0.9710
	Fast only	4.0 ± 0.2	2.6 ± 0.4	N/A	11.0 ± 0.2	0.9695
C	Fast & slow	8.7 ± 0.9	1.7 ± 0.3	−0.73 ± 0.02	21.0 ± 0.4	0.9771
	Fast only	8.5 ± 0.4	1.8 ± 0.2	N/A	21.0 ± 0.4	0.9797

mono-exponential component which strongly suggests that their rate of production is kinetically controlled by the fast-rate phase. This means that the previously reported oxygen-centred free radicals, assumed to be generated in the fast-rate phase [4], are able to immediately abstract protons attached to benzyl rings to yield carbon-centred radicals. In contrast, since the subsequent consumption of these carbon-centred radicals appear to be much slower, it must be governed by the overall kinetics of the slow-rate phase. Once the system enters the slow-rate phase, the rate of oxygen-centred free radical production and thus carbon-centred radical production will become comparable to their rate of consumption, and therefore, as can be seen in Fig. 5a, no net increase in the amount of carbon-centred radicals is observed.

In line with these hypotheses, the k_f' values obtained for the radical production were within a similar range to those for sulfoxide production. Similarly, the k_f' for binder B was again the fastest, which suggests that both organic carbon-centred radicals and sulfoxide productions in the fast reaction may be controlled by the same rate-limiting process.

It is interesting to mention that, in contrast to FTIR results, the harsher oxidation effect was observed for binder C. This difference can be explained by the fact that binder C was the result of a visbreaking process, which is a mild cracking process, resulting in radical formation. This can explain the higher initial organic carbon-centred radical concentration observed in bitumen C (Fig. 5a).

In addition, the VO^{2+} signal appears to stay constant over the ageing time in Fig. 5b, for the three investigated binders. It can be exploited as an indicator of the vanadium content in petroleum [38]. Of particular interest is that this assignment seems to remain unaffected by ageing and could be potentially used as a marker for the origin of the bitumen.

Together the two spectroscopic techniques give strong evidence for the two rates of a dual-oxidation route. It is important to mention when comparing the two different spectroscopic techniques that efforts to lessen the effect of different film thickness were taken into account. Given this, FTIR supports that between 2 and 5 days for all the examined binders the fast-rate reaction has finished, whereas EPR proves that carbon-centred radicals, which is believed to be produced and subsequently consumed during the slow-rate phase, actually evolve with the fast-rate phase kinetics. The ageing time interval of 8 days was used afterwards for TOF-SIMS surface analyses to unravel the main products after the combined effects of the fast- and slow-rate phase.

3.2. Oxygenated products

TOF-SIMS was used to analyse molecular changes on the bitumen surfaces upon ageing. Positive and negative ion spectra were acquired for the three binders (A, B and C) in the unaged state and after 8 days of ageing, at which point the fast-rate phase is mainly completed and the slow-rate phase has been initiated. Representative spectra of the unaged and aged samples of bitumen A and C are presented in Fig. 6 and ion assignments of peaks relevant to ageing are listed in Tables 6 and 7. No clear changes due to ageing can be observed in the major peaks of the spectra, indicating that the effect of ageing on the molecular surface structure is relatively small. In contrast, clear differences can be observed between the spectra of bitumen A and C, mainly reflecting the wax content of bitumen C. As reported previously wax segregates effectively in bitumen to form a thin layer of wax, largely covering the surface, which can be observed in the spectra of bitumen C [28]. The higher intensities of peaks in bitumen C represent aliphatic species, whereas the spectrum of the wax-free bitumen A displays higher intensities of peaks representing aromatic species, as well as N- and S-containing organics.

Although the major peaks in the TOF-SIMS spectra are essentially unchanged, the effect of ageing can be observed by consideration of oxygen-containing fragment ions, including SO_x-, NO_x- and O_x-containing organic ions, which are present at lower signal intensities, mainly in the negative ion spectra (see Tables 6-7).

The oxygen-containing fragment ions of the three binders were analysed based on normalised signal intensities and categorised into SO_x-containing (Fig. 7a) and HO_x-containing fragments (Fig. 7b). A strong increase in the intensity of the fragments with the generic formula RSO_x and RHO_x can be observed, strongly indicating the formation of sulfoxide- and oxygen-related compounds as a result of ageing. Additionally, for all binders the amount of cyanate fragments, with generic formula RNO^-, also increased during oxidation. It is important to note here that signal intensities of different ions should not be compared to indicate concentration differences between the corresponding molecular species, as the yield of formation for different ions may vary considerably. Instead, signal intensities of the same ion can be compared to indicate concentration differences between samples of the specific species that it represents.

Table 6
Utilised oxygenated peaks for negative ions of TOF-SIMS.

Ion	Observed mass (m/z)	Assignment of molecular structure
O^-	15.994	O_x-containing
OH–	17.004	HO_x-containing
CN^-	26.003	N-containing
$C_3H_2^-$	38.016	Aliphatic
$C_3H_3^-$	39.024	Aliphatic
C_2HO^-	41.006	HO_x-containing
CNO^-	42.002	NO_x-containing
CHO_2^-	45.001	HO_x-containing
$C_4H_3^-$	51.023	Aliphatic
CSO^-	59.967	SO_x-containing
SO_2^-	63.963	SO_x-containing
C_4HO^-	65.003	HO_x-containing
$C_5H_5^-$	65.038	Aliphatic
$C_2H_3SO^-$	74.989	SO_x-containing
$C_6H_5^-$	77.037	Aliphatic
SO_3^-	79.961	SO_x-containing
SO_4H^-	95.959	SO_x-containing
C_3NO^-	96.999	NO_x-containing

Table 7
Utilised oxygenated peaks for positive ions of TOF-SIMS.

Ion	Observed mass (m/z)	Assignment of molecular structure
CH_3O^+	31.020	O_x-containing
$C_3H_5^+$	41.047	Aliphatic
$C_2H_3O^+$	43.020	O_x-containing
$C_3H_7^+$	43.066	Aliphatic
$C_4H_7^+$	55.068	Aliphatic
$C_4H_9^+$	57.087	Aliphatic
$C_3H_7O^+$	59.049	O_x-containing
$C_5H_7^+$	67.066	Aliphatic
$C_5H_9^+$	69.087	Aliphatic
$C_5H_{11}^+$	71.117	Aliphatic
$C_6H_9^+$	81.087	Aliphatic
$C_6H_{11}^+$	83.112	Aliphatic
$C_6H_{13}^+$	85.135	Aliphatic
$C_7H_{11}^+$	95.106	Aliphatic
$C_7H_{13}^+$	97.129	Aliphatic
$C_8H_{13}^+$	109.128	Aliphatic
$C_9H_7^+$	115.059	Aromatic
$C_9H_{11}^+$	119.105	Aliphatic
$C_{10}H_8^+$	128.068	Aromatic
$C_{13}H_9^+$	165.079	Aromatic

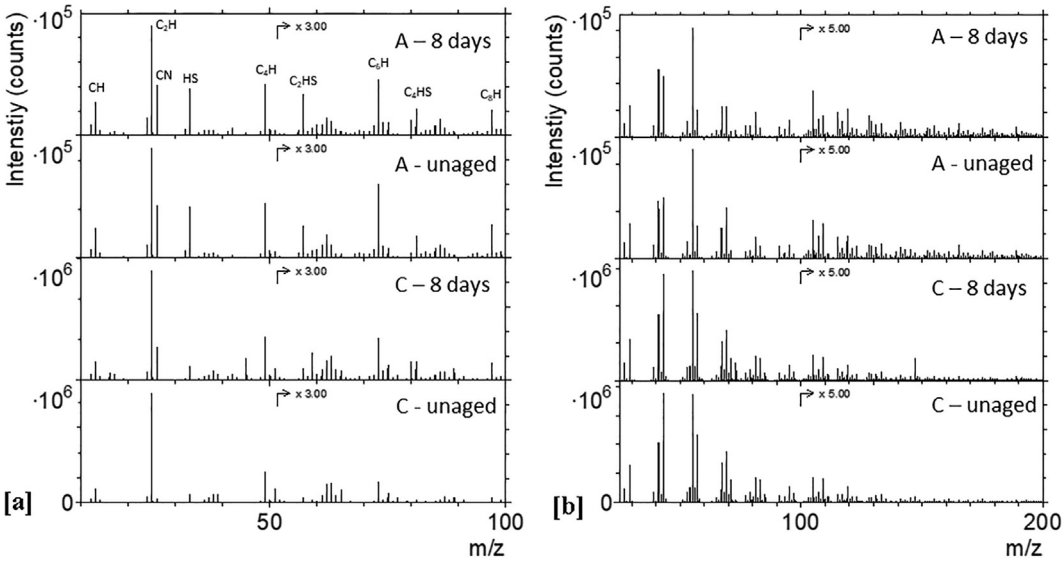

Fig. 6. Negative [a] and positive [b] ion spectra of bitumen A and C before and after M–TFOT ageing for 8 days.

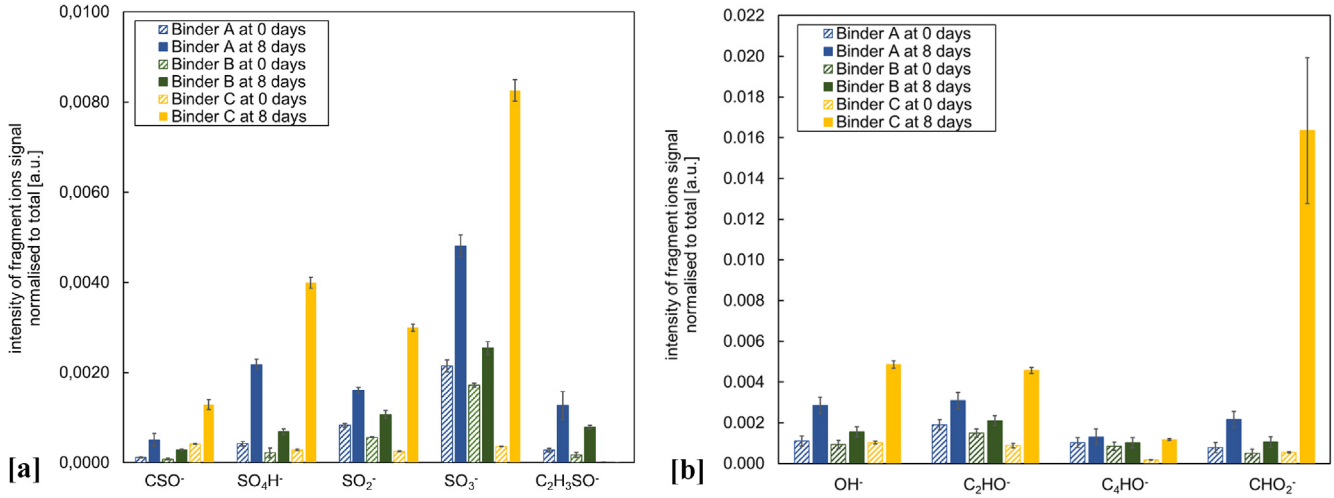

Fig. 7. Intensity of SO_x-containing [a] and HO_x-containing compounds via TOF-SIMS for all three binders [b]. Mean values from three measurements are presented and error bars are +/- 1 standard deviation.

Comparing the different bitumens, the effect of ageing is generally higher for bitumen A compared to bitumen B, but the strongest effect is observed for the wax-containing bitumen C. Furthermore, bitumen A and B show no effect of ageing on the intensities of fragment ions without oxygen content, including CN^- and aliphatic/aromatic hydrocarbon fragments. For bitumen C, however, ageing results in increased intensities of CN^- (Fig. 8), as well as in hydrocarbon fragments representing aromatic species, and decreased intensities of aliphatic hydrocarbon fragment ions, see Fig. 9.

Next to sulfoxide formation during the slow reaction, alcohol groups may also be produced [4,39]. The sulfoxide intensity observed with FTIR has been assigned, up to now, completely to this functional group. However, an overlap with other HO_x-containing groups may exist in the corresponding infrared absorption band (around 1100 cm^{-1}), indicating that alcohols and sulfoxides may coincide. Whereas the origin of the increase of this infrared absorption band upon ageing, therefore, is unknown, the observed increase of HO_x-containing fragments with TOF-SIMS is consistent with the formation of alcohols and/or carboxylic acids. It can thus be speculated that ageing results in the formation of more polar species, e.g. alcohols or carboxylic acids, which then

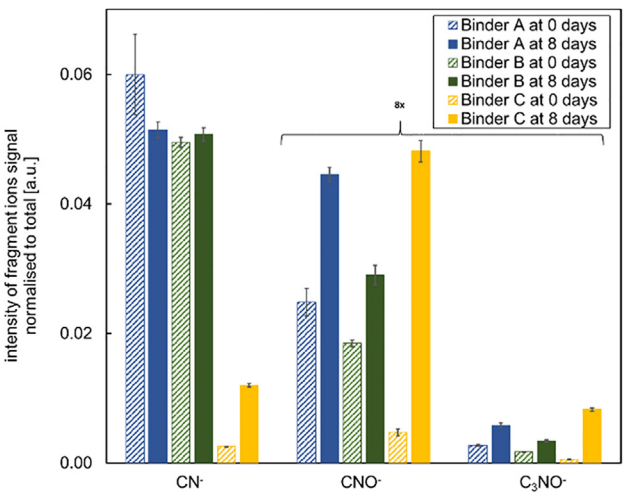

Fig. 8. Intensity of nitrogen-containing compounds.

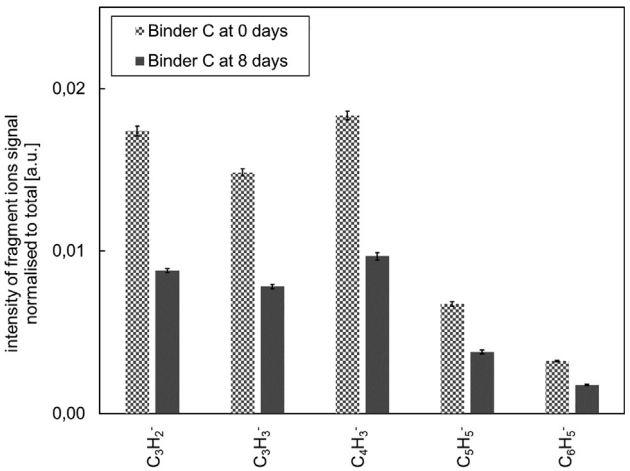

Fig. 9. Negative ions of binder C assigned to aliphatics.

may affect the molecular interactions and eventually the rheology of bitumen.

Previously [40,41], it was found that nitrogen-containing compounds can be identified in oxidised bitumens without significantly changing upon ageing [6]. In this study, the increase of RNO^- fragments indicates that additional oxidation products, those of nitrogen-containing compounds are present upon ageing, which should be taken into account in a future oxidation scheme. It can also be expected that the concentration of the different heteroatoms may have an impact on the intensity of the different fragments.

In Fig. 10, TOF-SIMS spectra of bitumen C are presented at a higher mass range, m/z 350–1200, where the peaks to a larger extent correspond to intact or nearly intact molecular species. The envelope of peaks at m/z 500–1000 in both negative and positive ion spectra can be assigned to intact wax molecules, as previously articulated by Lu [28], for which the intensity reduction upon ageing is consistent with the reduced intensities of the aliphatic fragment ions upon ageing (Fig. 9). Interestingly, ageing of bitumen C produces a new envelope of peaks at m/z 600–800 in the negative ion spectrum. Although unambiguous identification of these peaks is not possible due to the limited mass resolution, a mass separation of m/z = 14 between equivalent peaks and the exact mass of

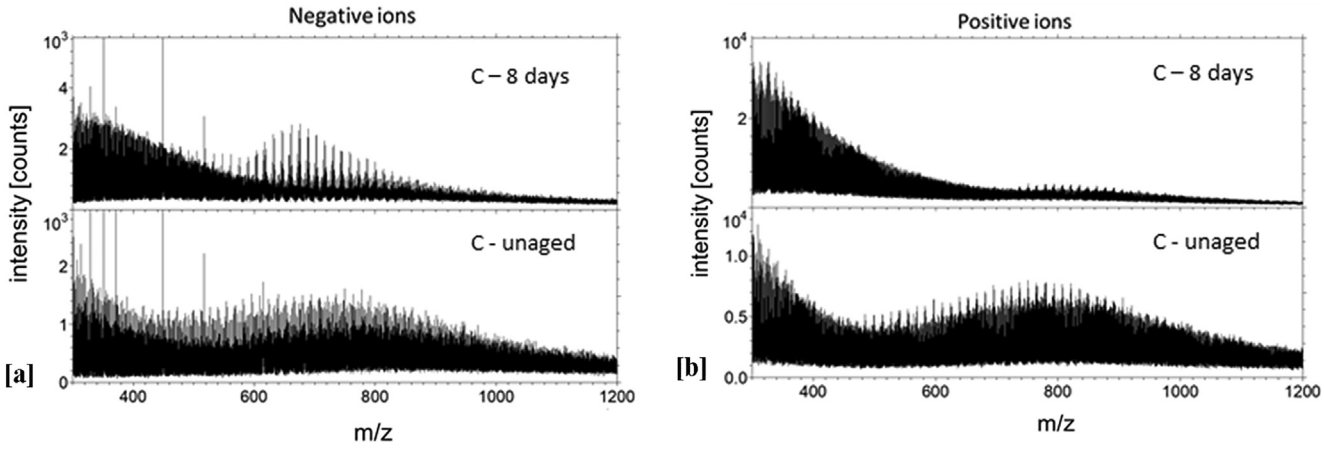

Fig. 10. High mass range of negative [a] and positive ion spectra of bitumen C before and after M–TFOT ageing for 8 days [b].

the peaks is consistent with molecules comprised of nearly saturated aliphatic hydrocarbon chains with an added SO_x functional group. For example, a peak observed at *m/z* 689.63 is consistent with $C_{45}H_{85}SO_2$, containing both an aliphatic and a small aromatic structure in which the S = O may be included. The latter may be taken as a consequence of oxidation and its subsequent sulfoxide formation.

For the positive ions, the effect of ageing was mainly observable in binder C. A clear increase in the intensities of O-containing organic ions was observed, reflecting the formation of oxidation products on the bitumen surface (Fig. 11). Furthermore, positive ions of aliphatic fragments show a decreasing trend as can be seen in Fig. 11, in contrast to polycyclic aromatic hydrocarbons (PAH) which increase upon ageing (Fig. 12), consistent with the observations for the negative ions (Fig. 9).

Finally, in order to investigate the spatial distribution of the wax fraction and the ageing-related molecular species on the surface of bitumen C, high-resolution TOF-SIMS images were generated (Fig. 13). A clear phase separation with a governing aliphatic phase is observed, with particles about 5–10 μm in size which covered most of the surface. Apparent wax-related particles (represented by aliphatics) cover most part of the surface and the spaces between these particles display increased signal intensities of ageing-related ions, such as O^-. CN^- and $(H)SO_x^-$ (Fig. 13), as well as aromatics (not shown here).

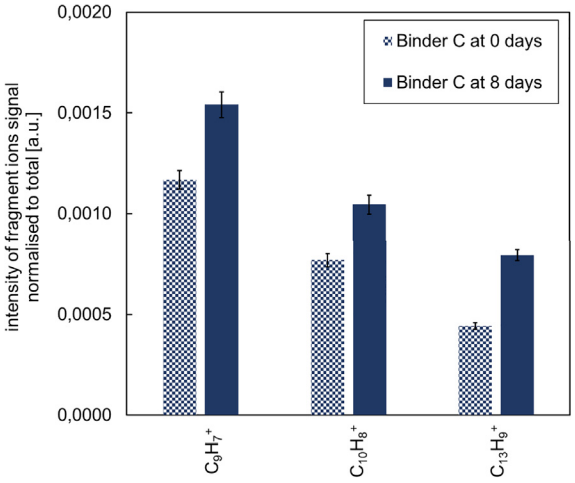

Fig. 12. Intensity of PAH fragments in selected positive ions.

4. Conclusions

In this work, the oxidative ageing mechanisms of three binders were investigated by FTIR, EPR and TOF SIMS. Binders were aged with modified thin-film oven test at a temperature of 50 °C. Consis-

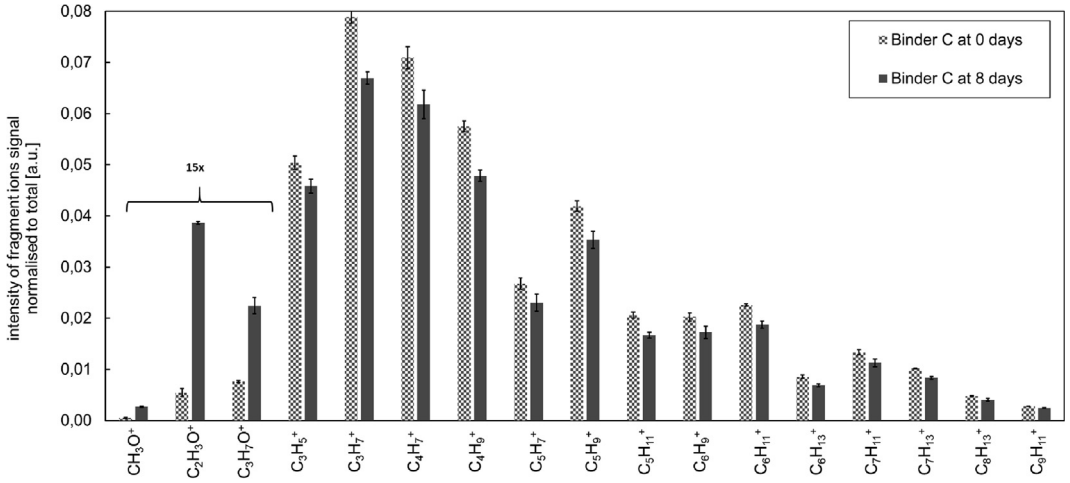

Fig. 11. Intensity of O-containing and aliphatic fragments in selected positive ions.

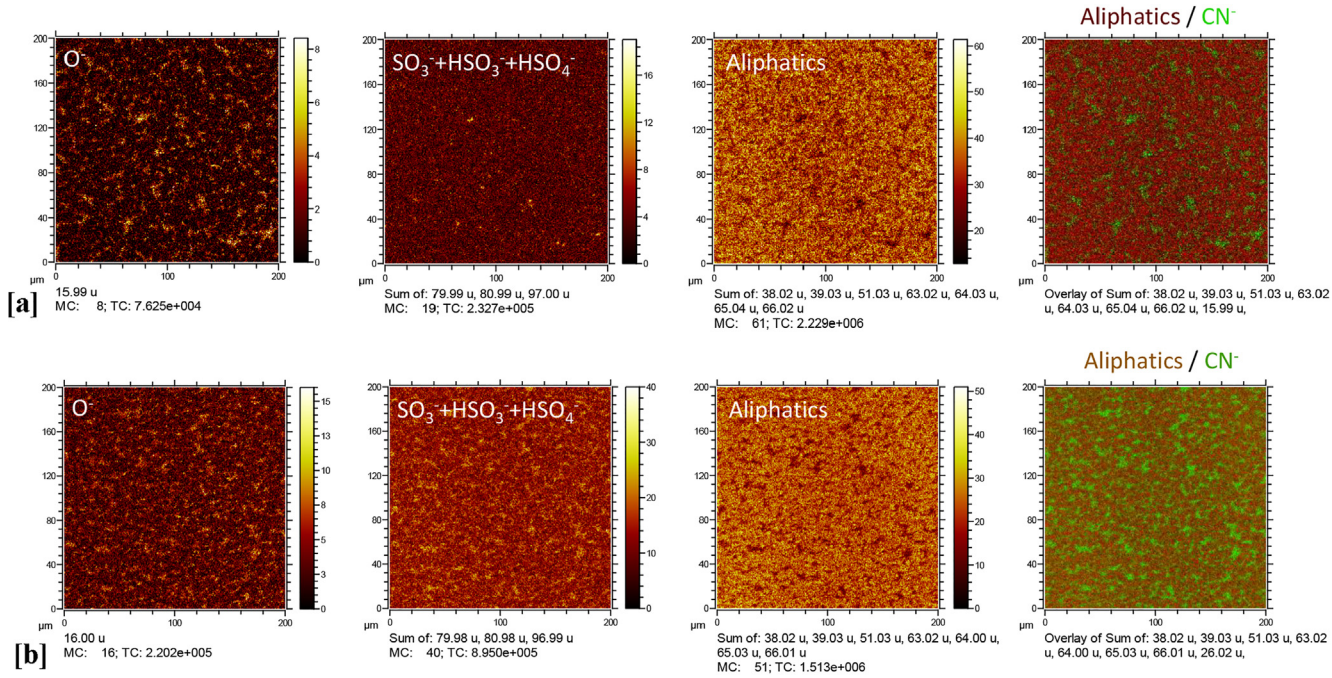

Fig. 13. High-resolution TOF-SIMS images of selected negative fragment ions on the surface of bitumen C before [a] and after ageing [b]. The signal intensities in the images are given as the maximum number of ion counts per pixel (MC) and total ion counts in the entire image (TC).

tent with previous studies the results from FTIR support the existence of two rate-determining oxidation phases, a fast- and a slow-rate and a rapid sulfoxide formation during the fast. For the examined binders this transition point was found to be between 2 and 5 days. Synchronous EPR measurements demonstrate that the overall amount of organic carbon-centred radicals evolves with the fast-rate phase. Taken together, the findings of the FTIR and TOF-SIMS spectrometry indicate that sulfoxide-, nitrogen- and oxygen-containing compounds, e.g. alcohols and/or carboxylic acids, are formed after the occurring fast- and slow-rate phases. An increase of aromatics and the accompanied decrease of aliphatics was only observed for the wax-containing binder.

Overall, the insights gained from this study may be particularly interesting for laying the groundwork for future research into the underlying oxidation mechanisms in bitumen. Future work could include more binder types or different ageing conditions. Of particular interest could be to investigate whether standardised accelerated ageing simulations would induce similar changes as observed in this study using a representative temperature.

CRediT authorship contribution statement

Georgios Pipintakos: Methodology, Investigation, Validation, Formal analysis, Writing - original draft. **H.Y. Vincent Ching:** Software, Formal analysis, Investigation, Validation, Writing - review & editing. **Hilde Soenen:** Conceptualization, Supervision, Writing - review & editing. **Peter Sjövall:** Formal analysis, Investigation, Writing - review & editing. **Uwe Mühlich:** Supervision, Writing - review & editing. **Sabine Van Doorslaer:** Conceptualization, Writing - review & editing. **Aikaterini Varveri:** Writing - review & editing. **Wim Van den bergh:** Writing - review & editing. **Xiaohu Lu:** Conceptualization, Writing - review & editing.

Declaration of Competing Interest

The authors declare that they have no known competing financial interests or personal relationships that could have appeared to influence the work reported in this paper.

Acknowledgements

The authors gratefully acknowledge support from Nynas AB and the European Union for H.Y. Vincent Ching's H2020-MSCA-IF grant (grant number 792946. iSPY).

References

[1] J.S. Moulthrop, M. Massoud, The SHRP Materials Reference Library, Washington DC, 1993
[2] X. Lu, P. Sjövall, H. Soenen, Structural and chemical analysis of bitumen using time-of-flight secondary ion mass spectrometry (TOF-SIMS), Fuel. 199 (2017) 206–218, https://doi.org/10.1016/j.fuel.2017.02.090.
[3] J.C. Petersen, R.E. Robertson, J.F. Branthaver, P.M. Harnsberger, J.J. Duvall, S.S. Kim, H.U. Bahia, R. Dongre, C.E. Antle, M.G. Sharma, Binder Characterization and Evaluation Volume 4 : Test M ethods, Washington DC, 1994.
[4] J.C. Petersen, R. Glaser, Asphalt Oxidation Mechanisms and the Role of Oxidation Products on Age Hardening Revisited, Road Mater. Pavement Des. 12 (2011) 795–819, https://doi.org/10.1080/14680629.2011.9713895.
[5] L.M. De Carvalho, C.S. Grassmann, C. Paulo, D. Bohrer, A.C. Fröhlich, C.K. Hoinacki, F.R. Adolfo, L.E. Claussen, M. Cravo, L.F.M. Leite, Distribution of sulfur compounds in Brazilian asphalt cements and its relationship to short-term and long-term aging processes, Constr. Build. Mater. 117 (2016) 72–79, https://doi.org/10.1016/j.conbuildmat.2016.04.111.
[6] J.C. Petersen, A Review of the Fundamentals of Asphalt Oxidation (E-C140), Transp. Res. Rec. J. Transp. Res. Board. (2009). https://doi.org/10.17226/23002
[7] J. Knotnerus, Oxygen uptake by bitumen solutions as a potential measure of bitumen durability, Am. Chem. Soc. Div. Pet. Chem. 16 (1971) D37–D59.
[8] T. Mill, The role of hydroaromatics in oxidative aging in asphalt, ACS Div. Fuel Chem. Prepr. 41 (1996) 1245–1248.
[9] G. King, Oxycyclics : Understanding catalyzed oxidation mechanisms in bitumen and other petroleum products, Fuel Sci. Technol. Int. 11 (1993) 201–238, https://doi.org/10.1080/08843759308916063.
[10] P. Herrington, B. James, T.F.P. Henning, Validation of a Bitumen Oxidation Rate Model, Transp. Res. Rec. J. Transp. Res. Board. 2632 (2017) 110–118, https://doi.org/10.3141/2632-12.
[11] J. Petersen, P. Harnsberger, Asphalt Aging: Dual Oxidation Mechanism and Its Interrelationships with Asphalt Composition and Oxidative Age Hardening, Transp. Res. Rec. J. Transp. Res. Board. 1638 (1998) 47–55, https://doi.org/10.3141/1638-06.
[12] P.R. Herrington, Diffusion and reaction of oxygen in bitumen films, Fuel. 94 (2012) 86–92, https://doi.org/10.1016/j.fuel.2011.12.021.
[13] P.K. Das, R. Balieu, N. Kringos, B. Birgisson, On the oxidative ageing mechanism and its effect on asphalt mixtures morphology, Mater. Struct. 48 (2014) 3113–3127, https://doi.org/10.1617/s11527-014-0385-5.
[14] B. Hofko, L. Porot, A.F. Cannone, L. Poulikakos, L. Huber, X. Lu, H. Grothe, K. Mollenhauer, FTIR spectral analysis of bituminous binders : reproducibility

and impact of ageing temperature, Mater. Struct. 51 (2018), https://doi.org/10.1617/s11527-018-1170-7.
[15] L.D. Poulikakos, C.F. A, D. Wang, L. Porot, B. Hofko, Impact of asphalt aging temperature on chemomechanics, RSC Adv. 9 (2019) 11602–11613. https://doi.org/10.1039/C9RA00645A
[16] S.-C. Huang, H. Di Benedetto, Advances in Asphalt, Materials (2015).
[17] R. Tauste, Understanding the bitumen ageing phenomenon : A review, Constr. Build. Mater. 192 (2018) 593–609, https://doi.org/10.1016/j.conbuildmat.2018.10.169.
[18] X. Lu, U. Isacsson, Effect of ageing on bitumen chemistry and rheology, Constr. Build. Mater. 16 (2002) 15–22, https://doi.org/10.1016/s0950-0618(01)00033-2.
[19] A. Dony, L. Ziyani, I. Drouadaine, S. Pouget, S. Faucon-Dumont, D. Simard, V. Mouillet, J.E. Poirier, T. Gabet, L. Boulange, A. Nicolai, C. Gueit, 1, MURE National Project : FTIR spectroscopy study to assess ageing of asphalt mixtures, in: 6th Eurasphalt Eurobitume Congr., 2016. https://doi.org/dx.doi.org/10.14311/EE.2016.154
[20] F.J. Ortega, F.J. Navarro, M. Jasso, L. Zanzotto, Physicochemical softening of a bituminous binder by a reactive surfactant (dodecenyl succinic anhydride, DSA), Constr. Build. Mater. 222 (2019) 766–775, https://doi.org/10.1016/j.conbuildmat.2019.06.117.
[21] J. Lamontagne, P. Dumas, V. Mouillet, J. Kister, Comparison by Fourier transform infrared (FTIR) spectroscopy of different ageing techniques : application to road bitumens, Fuel. 80 (2001) 483–488, https://doi.org/10.1016/S0016-2361(00)00121-6.
[22] G. Tarsi, A. Varveri, C. Lantieri, A. Scarpas, C. Sangiorgi, Effects of Different Aging Methods on Chemical and Rheological Properties of Bitumen, J. Mater. Civ. Eng. 30 (2018), https://doi.org/10.1061/(asce)mt.1943-5533.0002206.
[23] A. Vaitkus, A. Zofka, Evaluation of bitumen fractional composition depending on the crude oil type and production technology, in: 9th Int. Conf. Environ. Eng., 2014.
[24] P. Mikhailenko, H. Baaj, Comparison of Chemical and Microstructural Properties of Virgin and Reclaimed Asphalt Pavement Binders and Their Saturate, Aromatic, Resin, and Asphaltene Fractions, Energy & Fuels. 33 (2019) 2633–2640, https://doi.org/10.1021/acs.energyfuels.8b03414.
[25] K. Zhao, Y. Wang, F. Li, Influence of ageing conditions on the chemical property changes of asphalt binders, Road Mater. Pavement Des. (2019) 1–29, https://doi.org/10.1080/14680629.2019.1637771.
[26] P. Mikhailenko, C. Kou, H. Baaj, L. Poulikakos, A. Cannone-falchetto, J. Besamusca, B. Hofko, Comparison of ESEM and physical properties of virgin and laboratory aged asphalt binders, Fuel. 235 (2019) 627–638, https://doi.org/10.1016/j.fuel.2018.08.052.
[27] D. Grossegger, Microstructural aging of bitumen Microstructural aging of bitumen, in: 6th Eurasphalt Eurobitume Congr., 2016. https://doi.org/10.14311/EE.2016.135.
[28] X. Lu, P. Sjövall, H. Soenen, M. Andersson, Microstructures of bitumen observed by environmental scanning electron microscopy (ESEM) and chemical analysis using time-of- flight secondary ion mass spectrometry (TOF-SIMS), Fuel. 229 (2018) 198–208, https://doi.org/10.1016/j.fuel.2018.05.036.
[29] J.P. Aguiar-moya, J. Salazar-delgado, A. García, A. Baldi-, V. Bonilla-mora, L.G. Loría-salazar, J. Salazar-delgado, A. García, A. Baldi-, Effect of ageing on micromechanical properties of bitumen by means of atomic force microscopy, Road Mater. Pavement Des. 18 (2017) 203–215, https://doi.org/10.1080/14680629.2017.1304249.
[30] Y. Cui, C.J. Glover, J. Braziunas, H. Sivilevicius, Further exploration of the pavement oxidation model Diffusion-reaction balance in asphalt, Constr. Build. Mater. 161 (2018) 132–140, https://doi.org/10.1016/j.conbuildmat.2017.11.095.
[31] R. Karlsson, U. Isacsson, Laboratory studies of diffusion in bitumen using markers, J. Mater. Sci. 38 (2003) 2835–2844, https://doi.org/10.1023/A:1024476217060.
[32] R. Han, X. Jin, C.J. Glover, Petroleum Science and Technology Oxygen Diffusivity in Asphalts and Mastics, Pet. Sci. Technol. (2013) 37–41, https://doi.org/10.1080/10916466.2011.559506.
[33] A. Stoll , S.; Schweiger, EasySpin, a comprehensive software package for spectral simulation and analysis in EPR, J. Magn. Reson. 178 (2006) 42–55. https://doi.org/https://doi.org/10.1016/j.jmr.2005.08.013
[34] M. Espinosa; P.A. Camper; R. Salcedo, Electron Spin Resonance and Electronic Structure of Vanadyl−Porphyrin in Heavy Crude Oils, Inorg. Chem. 40 (2001) 4543–4549. https://doi.org/https://doi.org/10.1021/ic000160b
[35] L.G. Gilinskaya, EPR spectra of V(IV) complexes and the structure of oil porphyrins, J. Struct. Chem. 49 (2008) 245–254, https://doi.org/10.1007/s10947-008-0120-6.
[36] N.S. Ramachandran, Vasanth; van Tol, Johan; McKenna, Amy M.; Rodgers, Ryan P. ; Alan G. Marshall, Ryan P. ; Dalal, High Field Electron Paramagnetic Resonance Characterization of Electronic and Structural Environments for Paramagnetic Metal Ions and Organic Free Radicals in Deepwater Horizon Oil Spill Tar Balls, Anal. Chem. 87 (2015) 2306–2313. https://doi.org/10.1021/ac504080g
[37] V. Thiel, P. Sjövall, Time-of-Flight Secondary Ion Mass Spectrometry (TOF-SIMS): Principles and Practice in the Biogeosciences, in: Princ. Pract. Anal. Tech. Geosci., Royal Society of Chemistry, 2015: pp. 122–170.
[38] J.H. Tannous, A. De Klerk, Quantification of the Free Radical Content of Oilsands Bitumen Fractions, Energy & Fuels. 33 (2019) 7083–7093, https://doi.org/10.1021/acs.energyfuels.9b01115.
[39] M.F. Libert, I. Walczak, Effect of radio-oxidative ageing and pH on the release of soluble organic matter from bitumen, in: Int. Conf. Sci. Res. Back-End Fuel Cycle 21. Century, France, 2000: pp. 1–4.
[40] G. Boczkaj, A. Przyjazny, M. Kamin, Characteristics of volatile organic compounds emission profiles from hot road bitumens, Chemosphere. 107 (2014) 23–30, https://doi.org/10.1016/j.chemosphere.2014.02.070.
[41] I.-H. Wang, J.L. Boucher, R.A. Romine, R.D. Rowlett, G.-D. Lei, Oxidation chemistry in asphalt, Fuel Sci. Technol. Int. 11 (1993) 1–28. https://doi.org/http://dx.doi.org/10.1080/08843759308916056